

On the modeling of shear bands formation in J_2 materials with damage evolution

Sebastián D'heres⁽¹⁾ and Eduardo N. Dvorkin^{(2)*}

⁽¹⁾Department of Mechanical Engineering, Instituto Tecnológico de Buenos Aires
Av. E. Madero 399

C1106ACD, Buenos Aires, Argentina

⁽²⁾Engineering School, University of Buenos Aires
Av. Las Heras 2214, C1127AAR Buenos Aires, Argentina
SIM&TEC

Av. Pueyrredón 2130, C1119ACR Buenos Aires, Argentina

Abstract

The strain localization in J_2 materials with damage evolution is modeled using embedded strong discontinuity modes. In this procedure an heuristic bandwidth scale is adopted to model the damage evolution in the shear bands. The bifurcation triggering conditions and band growth directions are studied for these materials.

The resulting formulation does not require a specific mesh refinement to model a localization, provides mesh independent results also insensitive to element distortions and allows to calibrate the model response using experimental data.

The formulation capability is shown embedding the strong discontinuity modes into quadrilateral and higher order elements.

Keywords: ductile fracture, plasticity, localization, shear band, strong discontinuity, multiple scales formulation.

1 Introduction

Ductile fracture is a complex phenomena normally preceded by a strong plastic deformation localized in a very narrow zone as schematically described in Fig. 1. This localized plastic deformation induces local material damage in the localization zones while the material outside these zones remains almost undamaged, see [Backofen, 1972], [Gurson, 1975], [Gurson, 1977], [Tvergaard et al., 1981], [Tvergaard, 1981], [Tvergaard, 1982], [Tvergaard and Needleman, 1981], [Hutchinson and Tvergaard, 1981] and [Needleman, 1989].

The use of standard finite elements to model the behavior of plastic localization zones presents the problem that the elements size imposes the band scale; producing therefore mesh dependent models. Some attempts to model ductile fracture using standard finite element techniques have been developed; in these attempts the

*Corresponding author. Email: edvorkin@simytec.com

mesh was graded according to micromechanical parameters, see [Batisse et al., 1987], [Ishikawa et al., 2000] and [Ishikawa et al., 2001].

In the modeling of ductile fracture there are two main issues:

- The simultaneous modeling of the localized plastic deformations and of the elastoplastic continua; that is to say, the modeling of multiple coexisting scales.
- The realistic description of the damage evolution in the material inside the band.

In what follows we summarize some of the techniques that were proposed in the literature for the multi-scale modeling of localization phenomena.

The enhancement of the strain fields used in the finite element formulation was discussed in [Ortiz et al., 1987], where a strain jump function was added to each element where the localization criteria was satisfied. Different enhancement techniques were also proposed in [Belytschko et al., 1988], [Simo et al., 1993], [Armero and Garikipati, 1996] [Armero and Garikipati, 1995] and [Sluys, 1997].

Discontinuous displacement fields were used to represent the strain jump across the band in the strong discontinuity approach, see [Oliver, 1996a], [Oliver, 1996b], [Oliver et al., 1999] and [Oliver and Huespe, 2004]. To model shear bands using this technique a specific strain softening material law was defined for the material inside the bands.

X-FEM techniques were used in [Moës et al., 1999], [Samaniego and Belytschko, 2005] and [Areias and Belytschko, 2006] among other references. In [Moës et al., 1999], for modeling crack opening, the discontinuities are represented enriching the finite element interpolations with a discontinuous field near the crack tip and adding an embedded traction separation law applied to cohesive surfaces. Focused on the modeling of shear bands, in [Samaniego and Belytschko, 2005] and [Areias and Belytschko, 2006], the enhancement was performed with a fine scale strain function.

Unfitted finite elements were used in [Hansbo and Hansbo, 2002], [Hansbo and Hansbo, 2004], [Mergheim et al., 2005] and [Mergheim et al., 2007] with additional degrees of freedom at the nodes belonging to the elements crossed by the bands. The material degradation inside the shear bands was modeled via a strain softening law and the cracks were opened dissipating the material fracture energy.

A sub-grid method with an inserted displacement discontinuity was used in [Yang et al., 2005] to model the development of adiabatic shear bands in dynamic problems.

A combination of X-FEM for the macroscale and FEM for the microscale was presented in [Belytschko et al., 2007]. This multiscale aggregating discontinuities method (MAD) excludes the subdomains with internal discontinuities from the coarser mesh and replaces them with an equivalent discontinuity to overcome instability using X-FEM. In the finer scale a unit cell is used to determine the behavior of the microscale under the loadings obtained from the larger scale. The multiple discontinuities existing in the microscale are aggregated into only one equivalent to be injected into the larger scale. For more details on the unit cell approach see [Feyel and Chaboche, 2000].

Regarding the modeling of the band damage evolution, the mechanisms inside the band, function of the material microstructure, need to be modeled using a mechanical-metallurgical coupling [Gilman, 1994].

In general, the mechanical properties of the localization zone are modeled using dissipative mechanisms [Armero, 2001]. More specifically, these dissipative mechanisms cannot be associated with material hardening, since no localization can arise in this case [Backofen, 1972]. Hence, the dissipative mechanism has been modeled using softening material laws, that although are thermodynamically unacceptable, see [Bažant, 1976] and [Ottosen, 1986], can be adjusted to available experimental data using a few parameters.

Other approaches that require more material experimental data but avoid the thermodynamic issue are the damage theory, see [Cervera et al., 2004] or the ductile pressure dilatant materials as the Gurson-Tvergaard-Needleman material model, used to model the material mechanical degradation, see [Gurson, 1975], [Gurson, 1977], [Tvergaard, 1981], [Tvergaard, 1982], [Tvergaard and Needleman, 1981] and [Sanchez et al., 2008].

In plane problems, a shear band can be characterized by a line with normal ${}^t\mathbf{n}$, the direction ${}^t\mathbf{m}$ of the displacement jump $[[{}^t\mathbf{u}]]$ and a scalar bandwidth d , as proposed in [Ottosen and Runesson, 1991] and [Larsson et al., 1993]; in our description of the problem we adopt $d = 0$ for the band topology. In Fig. 2 we draw a schematic representation of the above definitions, considering that the displacement jump in the shear band is along its tangential direction, as in the J_2 elastoplastic model [D’hers and Dvorkin, 2009].

The objective of the present paper is to extend the formulation developed in [D’hers and Dvorkin, 2009] to the modeling of J_2 material models that include damage evolution. The present work is based on:

- the formulation previously developed for modelling cracks in brittle materials using embedded localization lines, see [Dvorkin et al., 1990] and [Dvorkin and Assanelli, 1991], where a physical traction separation law that exactly represents the material fracture energy defines the localization scale;
- the extension of those ideas for the modeling of J_2 localization via the use of strong discontinuity modes embedded in the element formulation, that we developed in [D’hers and Dvorkin, 2009].

Even though we are not intending to describe the micromechanical behavior inside the shear bands, we know that the phenomena that takes place there is beyond the continuum mechanics hypothesis, since the band dimensions are in the granular size scale. For this reason, to model the band formation, we heuristically define a bandwidth to represent the above mentioned micro-scale evolution. The definition of this bandwidth allows the experimental calibration of the model and provides mesh independent results also insensitive to mesh distortions.

The paper is organized as follows: the shear bands triggering criterion is discussed in the second section, the finite element implementation, the localization modes and the heuristic bandwidth rule are described and discussed in the third section. In the fourth section we present the numerical implementation of our new formulation and discuss the numerical experimentation that we developed to test it; finally the conclusions are stated in the fifth section.

2 Shear bands triggering criterion

In the following set of equations we summarize the constitutive relation, the flow rule and the yield surface that is used in the J_2 associated plasticity model with isotropic hardening and considering infinitesimal strains, [Dvorkin and Goldschmit, 2005]

$${}^t\sigma_{ij} = {}^tC_{ijkl}^E ({}^t\varepsilon_{kl} - {}^t\varepsilon_{kl}^P) \quad (1a)$$

$${}^t\varepsilon_{kl}^P = {}^t\lambda \quad {}^t\left(\frac{\partial\Phi}{\partial\sigma_{kl}}\right) \quad (1b)$$

$${}^t\Phi = \frac{3}{2} {}^t s_{ij} {}^t s_{ij} - {}^t\sigma_y^2 = 0. \quad (1c)$$

In the above equations, written in a Cartesian coordinate system, ${}^t\sigma_{ij}$ are the components of the Cauchy stress tensor at time (configuration) t , ${}^tC_{ijkl}^E$ are the components of the fourth order elastic constitutive

tensor, ${}^t\varepsilon_{kl}$ are the components of the strain tensor, ${}^t\varepsilon_{kl}^P$ are the components of the plastic deformation tensor, ${}^t s_{ij}$ are the components of the deviatoric part of the Cauchy stress tensor, ${}^t\Phi = 0$ is the yield function and ${}^t\sigma_y$ is the yield stress.

It has been shown in [Rice, 1976] that the triggering of bifurcation in the material behavior and the respective band orientation can be determined from the singularity of the acoustic tensor. To determine the bifurcation conditions for J_2 softening materials we state its fourth order elastoplastic constitutive tensor, see [Simo and Hughes, 1997],

$$\underline{\underline{\underline{\underline{C}}}}^{\text{EP}} = \frac{2\nu G}{1-2\nu} \underline{\underline{\underline{\underline{g}}}} \underline{\underline{\underline{\underline{g}}}} + 2G \underline{\underline{\underline{\underline{I}}}} - \frac{6G^2}{3G + {}^tH} \frac{\underline{\underline{\underline{\underline{t}}}} \underline{\underline{\underline{\underline{t}}}}}{\underline{\underline{\underline{\underline{t}}}} : \underline{\underline{\underline{\underline{t}}}}} \quad (2)$$

where tH is the isotropic hardening modulus, $\underline{\underline{\underline{\underline{t}}}}$ is the deviatoric stress tensor, ν the Poisson ratio, G the elastic tangential modulus, and

$$\underline{\underline{\underline{\underline{I}}}} = \frac{1}{2} ({}^t g^{ik} {}^t g^{jl} + {}^t g^{il} {}^t g^{jk}) \underline{\underline{\underline{\underline{g}}}}_i \underline{\underline{\underline{\underline{g}}}}_j \underline{\underline{\underline{\underline{g}}}}_k \underline{\underline{\underline{\underline{g}}}}_l \quad (3)$$

is the symmetric fourth order identity tensor. In these equations we indicate the tensorial product between two tensors as $\underline{\underline{\underline{\underline{a}}}} \underline{\underline{\underline{\underline{b}}}}$ (in other references it is indicated as $\underline{\underline{\underline{\underline{a}}}} \otimes \underline{\underline{\underline{\underline{b}}}}$) and the number of underlines indicates the tensor order.

The isotropic hardening modulus, tH , can be defined as a function of the equivalent plastic strain,

$${}^t\bar{\varepsilon}^P = \sqrt{\frac{2}{3} {}^t\varepsilon_{kl}^P {}^t\varepsilon_{kl}^P} \quad (4)$$

and contains the information about the material damage evolution:

$${}^tH = {}^tH ({}^t\bar{\varepsilon}^P) . \quad (5)$$

We can calculate the determinant of the acoustic tensor using a convenient Cartesian coordinate system with base vectors ${}^t\hat{\underline{\underline{x}}}_i$ aligned with the band directions: ${}^t\hat{\underline{\underline{x}}}_1$ in the ${}^t\underline{\underline{n}}$ -direction and ${}^t\hat{\underline{\underline{x}}}_2$ in the ${}^t\underline{\underline{m}}$ -direction. Using this coordinate system we build the D function which is the determinant of the acoustic constitutive tensor, see [Rice, 1976],

$$D = \det \left({}^t\hat{\underline{\underline{x}}}_1 \cdot \underline{\underline{\underline{\underline{C}}}}^{\text{EP}} \cdot {}^t\hat{\underline{\underline{x}}}_1 \right) \quad (6)$$

Because the stress state is on the yield surface, ${}^t\Phi = 0$ in Eqn. (1c) we get,

$${}^t\hat{s}_{12}^2 + {}^t\hat{s}_{13}^2 = \frac{{}^t\sigma_y^2}{3} - ({}^t\hat{s}_{11}^2 + {}^t\hat{s}_{22}^2 + {}^t\hat{s}_{11} {}^t\hat{s}_{22} + {}^t\hat{s}_{23}^2) \quad (7)$$

Evaluating Eqn. (6) and using Eqn. (7) we get,

$$D = Q (Q_1 ({}^t\hat{s}_{22}^2 + {}^t\hat{s}_{11} {}^t\hat{s}_{22} + {}^t\hat{s}_{23}^2) + Q_2 {}^t\hat{s}_{11}^2 + Q_3) \quad (8)$$

where a set of constants that do not depend on the orientation of the coordinate system ${}^t\hat{\underline{\underline{x}}}_i$ have been used,

$$\begin{aligned}
Q &= \frac{G^3}{{}^t\sigma_y^4 (3G + {}^tH) (1 - 2\nu)} \\
Q_1 &= 18G(1 - \nu) \\
Q_2 &= 9G \\
Q_3 &= 2 {}^t\sigma_y^2 {}^tH (1 + \nu)
\end{aligned}$$

If we consider D as a function only of the stresses, keeping constant all other variables, we find that it is continuous function and that it has only one extremum where,

$${}^t\hat{s}_{11} = {}^t\hat{s}_{22} = {}^t\hat{s}_{23} = 0 \quad (9)$$

To explore this extremum we test the positive definiteness of $Hessian(D)$ using an arbitrary vector \underline{a} ,

$$\underline{a}^T \underline{\underline{Hessian(D)}} \underline{a} = \frac{Q}{18G} \left((1 - \nu) \left((a_1 + a_2)^2 + a_2^2 + 2a_3^2 \right) + \nu a_1^2 \right) > 0 \quad (10)$$

For the D function to vanish at any point or region it is enough that the value at the minimum is negative or at least null. The evaluation of D under conditions stated in Eqn. (9) results in the necessary condition for bifurcation,

$$D = \frac{2 {}^tH G^3 (1 + \nu)}{{}^t\sigma_y^2 (3G + H) (1 - 2\nu)} < 0 \quad (11)$$

where we find, as expected, that bifurcation is only possible in perfect plasticity or softening situations, ${}^tH \leq 0$, regardless of the band direction and of the stress state. A discussion on physical grounds over the impossibility of producing shear bands in a material with plastic hardening is presented in Ref. [Backofen, 1972]. The sufficient condition for bifurcating is that there must exist a direction ${}^t\underline{\mathbf{n}} \equiv {}^t\hat{\underline{\mathbf{x}}}_1$ where $D < 0$; hence, to determine the bifurcation inception we must establish the conditions that the stress state independent variables ${}^t\hat{s}_{11}$, ${}^t\hat{s}_{22}$ and ${}^t\hat{s}_{23}$ have to fulfill.

By doing a coordinates transformation and assuming ${}^t\hat{s}_{23} = 0$ we get,

$$\begin{aligned}
{}^t\hat{s}_{11} &= \cos(\beta)^2 {}^t s_{11} - \sin(2\beta) {}^t s_{12} + \sin(\beta)^2 {}^t s_{22} \\
{}^t\hat{s}_{22} &= \sin(\beta)^2 {}^t s_{11} + \sin(2\beta) {}^t s_{12} + \cos(\beta)^2 {}^t s_{22},
\end{aligned} \quad (12)$$

being β the angle between base vectors ${}^t\hat{\underline{\mathbf{x}}}_1$ and ${}^t\underline{\mathbf{x}}_1$.

We use the above in Eqn. (8) considering that since Eqn. (1c) holds we can obtain a D function depending only on two stress deviatoric components. We choose ${}^t s_{11}$ and ${}^t s_{22}$ as the independent ones and leave as dependent ${}^t s_{12}$. Thus we get the function,

$$D = D({}^t s_{11}, {}^t s_{22}, \beta) \quad (13)$$

We need to numerically analyze Eqn. (13), since we could not arrive to a closed form solution. For every combination of ${}^t s_{11}$ and ${}^t s_{22}$ we determine the β angle that minimizes D , and if $D_{\min} \leq 0$ then bifurcation is feasible. In Fig. 3 for the material parameters $E = 200GPa$, ${}^0\sigma_y = 600MPa$ and $\nu = 0.3$ we plot in the deviatoric space the zones where bifurcation is possible for a range of softening values. It can be

seen that the bifurcation feasibility for ${}^tH = 0$ coincides with maximum shear states as it was shown in [Armero and Garikipati, 1995] and [D’hers and Dvorkin, 2009]. As softening grows the localization zones widen while centered in the pure shear direction with its edges remaining parallel.

As it was mentioned above, the band direction when ${}^tH = 0$ coincides with the maximum shear one. In Fig. 4 for a softening tangent modulus ${}^tH = -0.1 \cdot E$ we plot for every bifurcation point in the deviatoric space, the angle between the maximum shear direction and the band direction. It can be clearly seen that the misalignment between the band and the maximum shear direction results very small ($< 1.7^\circ$).

This result justifies our adoption of a pure shear strong discontinuity mode, as it is explained in the next section.

3 Finite element formulation

3.1 Strong discontinuity modes

When the above defined localization indicator detects the triggering of a shear band, we split the element kinematics into a continuum scale contribution and a localized scale deformation mode. The localized deformation mode must be able to model a distortion along the band direction while preserving volume in order to fulfill the J_2 incompressible flow condition.

The continuum and the localized scales are related by the joint fulfillment of compatibility (only one displacement field) and equilibrium (Eqn. (31)); but, it is the localized kinematics the one that models the shear band development and not the complete element kinematics as in the standard finite element formulations.

For an infinitesimal strain incremental analysis, the deformation increment is decomposed into elastic and plastic components; while the elastic deformation only contributes to the continuum scale, the plastic deformation contributes to the continuum and to the localized scales,

$$\underline{\underline{\varepsilon}} = \underline{\underline{\varepsilon}}^E + \underline{\underline{\varepsilon}}^P = \underline{\underline{\varepsilon}}_{cont}^E + \underline{\underline{\varepsilon}}_{cont}^P + \underline{\underline{\varepsilon}}_{loc}^P. \quad (14)$$

Since the equilibrium configuration at t is known, we can write the incremental relations,

$${}^{t+\Delta t}\underline{\underline{\varepsilon}} = \underline{\underline{\varepsilon}} + {}^t\underline{\underline{\varepsilon}} \quad (15a)$$

$${}^{t+\Delta t}\underline{\underline{u}} = \underline{\underline{u}} + {}^t\underline{\underline{u}}. \quad (15b)$$

With the purpose of dealing with the two aforementioned scales we split the increment of the nodal element displacement vector,

$${}^{t+\Delta t}\underline{\underline{\mathbf{U}}} - {}^t\underline{\underline{\mathbf{U}}} = \underline{\underline{\mathbf{U}}} \quad (16)$$

into a part that models the continuum scale and a part that models the localized scale; for both we use the interpolation matrix $\underline{\underline{\mathbf{H}}}$ ([Bathe, 1996]). Hence,

$$\underline{\underline{u}} = \underline{\underline{u}}_{cont} + \underline{\underline{u}}_{loc} = \underline{\underline{\mathbf{H}}} \underline{\underline{\mathbf{U}}} = \underline{\underline{\mathbf{H}}} \underline{\underline{\mathbf{U}}}_{cont} + \underline{\underline{\mathbf{H}}} \underline{\underline{\mathbf{U}}}_{loc}. \quad (17)$$

The localized nodal displacements have to reproduce the band kinematics; hence, following [D’hers and Dvorkin, 2009] we define,

$$\underline{\underline{u}}_{loc} = \underline{\underline{\mathbf{H}}} \underline{\underline{\mathbf{U}}}_{loc} = \underline{\underline{\mathbf{H}}} \gamma \underline{\underline{\Theta}} \quad (18)$$

where $\underline{\Theta}$ are the nodal displacements corresponding to the localized deformation mode to be defined later in this work and γ is the increment of a scalar parameter which is part of the problem unknowns. The incremental formulation for the parameter γ is,

$${}^{t+\Delta t}\gamma = \gamma + {}^t\gamma \quad (19)$$

Therefore,

$$\underline{u} = \underline{\mathbf{H}} \underline{\mathbf{U}} = \underline{\mathbf{H}} (\underline{\mathbf{U}} - \gamma \underline{\Theta}) + \underline{\mathbf{H}} \gamma \underline{\Theta} \quad (20)$$

Thus the resulting strain fields are, using Voight notation,

$$\underline{\varepsilon}_{cont} = \underline{\varepsilon}_{cont}^E + \underline{\varepsilon}_{cont}^P = \underline{\mathbf{B}} (\underline{\mathbf{U}} - \gamma \underline{\Theta}) \quad (21)$$

$$\underline{\varepsilon}_{loc} = \underline{\varepsilon}_{loc}^P = \underline{\mathbf{B}} \underline{\mathbf{U}}_{loc} = \underline{\mathbf{B}} \gamma \underline{\Theta} \quad (22)$$

where $\underline{\mathbf{B}}$ is the element strain-displacement matrix ([Bathe, 1996]).

The $\underline{\Theta}$ mode has to have its maximum distortional deformation aligned to the band angle β and must not introduce a volume change ¹,

$$\frac{\varepsilon_{loc4}}{\varepsilon_{loc1} - \varepsilon_{loc2}} = \tan\left(2\beta + \frac{\pi}{2}\right) \quad (23)$$

$$\varepsilon_{loc1} + \varepsilon_{loc2} + \varepsilon_{loc3} = 0 \quad (24)$$

To build $\underline{\Theta}$ for 2D elements, we consider that any $N - node$ quadrilateral element formulated in the isoparametric natural element space (r, s) has $2N$ eigenmodes among which there are: one volume change mode and two pure shear modes, as represented in Fig 5. By linearly combining those modes we can construct a "shear base" so as to obtain a pure shear mode in any desired direction. In Table I, for a 4 - Node bilinear element, we define the deformed element nodal coordinates corresponding to the three eigenmodes in the "shear base". For the case of higher order elements the ${}^t\Phi_r$ and ${}^t\Phi_s$ values for the additional nodes are obtained by interpolation of the corner node values:

	${}^t\Phi_r^1$	${}^t\Phi_s^1$	${}^t\Phi_r^2$	${}^t\Phi_s^2$	${}^t\Phi_r^3$	${}^t\Phi_s^3$	${}^t\Phi_r^4$	${}^t\Phi_s^4$
${}^t\Phi_I$	$\frac{1}{2}$	$\frac{3}{2}$	$-\frac{1}{2}$	$\frac{3}{2}$	$-\frac{1}{2}$	$-\frac{3}{2}$	$\frac{1}{2}$	$-\frac{3}{2}$
${}^t\Phi_{II}$	$\frac{3}{2}$	$\frac{3}{2}$	$-\frac{1}{2}$	$\frac{1}{2}$	$-\frac{3}{2}$	$-\frac{3}{2}$	$\frac{1}{2}$	$-\frac{1}{2}$
${}^t\Phi_{III}$	$\frac{3}{2}$	$\frac{3}{2}$	$-\frac{3}{2}$	$\frac{3}{2}$	$-\frac{3}{2}$	$-\frac{3}{2}$	$\frac{3}{2}$	$-\frac{3}{2}$

Table I. Nodal coordinates in the (r, s) natural system for the three eigenmodes that constitute the "shear base"

Using the three sets of nodal coordinates displayed in Table I and the unstrained nodal coordinates (r^k, s^k) we define three orthogonal nodal displacement vectors,

$${}^t\underline{\Psi}_A^k = [({}^t\Phi_A^k)_r - r^k] \underline{\mathbf{e}}_r + [({}^t\Phi_A^k)_s - s^k] \underline{\mathbf{e}}_s. \quad (25)$$

¹The strain components in the xy plane for plane problems are:

- for plane stress cases $\underline{\varepsilon}^T = [\varepsilon_1 \quad \varepsilon_2 \quad \varepsilon_4] = [\varepsilon_{xx} \quad \varepsilon_{yy} \quad 2\varepsilon_{xy}]$,
- for plane strain and axisymmetric cases $\underline{\varepsilon}^T = [\varepsilon_1 \quad \varepsilon_2 \quad \varepsilon_3 \quad \varepsilon_4] = [\varepsilon_{xx} \quad \varepsilon_{yy} \quad \varepsilon_{zz} \quad 2\varepsilon_{xy}]$

In the above equation ($\underline{\mathbf{e}}_r; \underline{\mathbf{e}}_s$) are orthonormal base vectors shown in Fig. 5 along the (r, s) natural directions; the subindex $A = I \dots III$ indicates the deformation mode and the upper index $k = 1 \dots N$ indicates the node.

In the (x_1, x_2) coordinate system we generalize Eqn. (25) using,

$${}^t \underline{\Psi}_A^k = \left[h_j \left(({}^t \Phi_A^k)_r, ({}^t \Phi_A^k)_s \right) x_i^j - x_i^k \right] \underline{\mathbf{e}}_i. \quad (26)$$

Inside the isoparametric element the displacements corresponding to the "shear base" modes are interpolated as,

$${}^t \underline{\Psi}_A = h_k {}^t \underline{\Psi}_A^k \quad (27)$$

where the h_k are the isoparametric interpolation functions ([Bathe, 1996]).

We compute the strain components at the element center from the three modes defined above,

$$\underline{\boldsymbol{\varepsilon}}_I = \underline{\mathbf{B}}_c \underline{\Psi}_I \quad (28a)$$

$$\underline{\boldsymbol{\varepsilon}}_{II} = \underline{\mathbf{B}}_c \underline{\Psi}_{II} \quad (28b)$$

$$\underline{\boldsymbol{\varepsilon}}_{III} = \underline{\mathbf{B}}_c \underline{\Psi}_{III} \quad (28c)$$

where $\underline{\mathbf{B}}_c = \underline{\mathbf{B}}(x_1^o, x_2^o)$ is the strain-displacements matrix calculated at the element center. The linear combination of the above defined strain fields results in the shear band localization strains $\underline{\boldsymbol{\varepsilon}}_{loc}$, where β_I , β_{II} and β_{III} are constant parameters to be determined,

$$\underline{\boldsymbol{\varepsilon}}_{loc} = \beta_I \underline{\boldsymbol{\varepsilon}}_I + \beta_{II} \underline{\boldsymbol{\varepsilon}}_{II} + \beta_{III} \underline{\boldsymbol{\varepsilon}}_{III} = \underline{\mathbf{B}}_c (\beta_I \underline{\Psi}_I + \beta_{II} \underline{\Psi}_{II} + \beta_{III} \underline{\Psi}_{III}) \quad (29)$$

To calculate β_I , β_{II} and β_{III} , we request that the strains $\underline{\boldsymbol{\varepsilon}}_{loc}$ fulfill Eqns. (23) and (24) together with the condition that if $\underline{\boldsymbol{\varepsilon}}_I$ and $\underline{\boldsymbol{\varepsilon}}_{II}$ are incompressible modes, $\beta_{III} = 0$ since no volume correction is required to satisfy the incompressibility condition ; if $\underline{\boldsymbol{\varepsilon}}_I$ and $\underline{\boldsymbol{\varepsilon}}_{II}$ are not incompressible modes we adopt $\beta_{III} = 1$.

Using the β_I , β_{II} and β_{III} parameters we compose a normalized $\underline{\Theta}$ mode,

$$\underline{\Theta} = \frac{\beta_I \underline{\Psi}_I + \beta_{II} \underline{\Psi}_{II} + \beta_{III} \underline{\Psi}_{III}}{|\beta_I \underline{\Psi}_I + \beta_{II} \underline{\Psi}_{II} + \beta_{III} \underline{\Psi}_{III}|} \quad (30)$$

3.2 Equilibrium iterative scheme

For the body shown in Fig. 6, in equilibrium at time t , and considering that a shear band has already been triggered, we seek the equilibrium configuration for time $t + \Delta t$, via the principle of virtual work. For a "material nonlinear only analysis" (geometrically linear analysis) ([Bathe, 1996]) we get, using the notation in Fig. 6,

$$\int_V \delta [\underline{\boldsymbol{\varepsilon}}_{cont}]^T {}^{t+\Delta t} \underline{\boldsymbol{\sigma}}_{cont} dv + \delta \underline{\mathbf{u}}_{loc}^T {}^{t+\Delta t} \underline{\mathbf{F}}_{loc} = \int_S \delta \underline{\mathbf{u}}^T {}^{t+\Delta t} \underline{\mathbf{p}} ds. \quad (31)$$

For the continuum,

$${}^{t+\Delta t} \underline{\boldsymbol{\sigma}}_{cont} = {}^t \underline{\boldsymbol{\sigma}}_{cont} + {}^t \underline{\mathbf{C}}^{\text{EP}} \underline{\mathbf{B}} (\underline{\mathbf{U}} - \gamma \underline{\Theta}). \quad (32)$$

Replacing Eqns. (17), (18), (21) and (32) in Eqn. (31) and since $\delta\mathbf{U}$ and $\delta\gamma$ are arbitrary variations we get, after some algebra,

$$\begin{bmatrix} {}^t\mathbf{K}_u & - {}^t\mathbf{K}_u \mathbf{\Theta} \\ - \mathbf{\Theta}^T {}^t\mathbf{K}_u & \mathbf{\Theta}^T {}^t\mathbf{K}_u \mathbf{\Theta} \end{bmatrix} \begin{bmatrix} \mathbf{U} \\ \gamma \end{bmatrix} = \begin{bmatrix} {}^{t+\Delta t}\mathbf{R} - {}^t\mathbf{F} \\ \mathbf{\Theta}^T ({}^t\mathbf{F} - {}^t\mathbf{F}_{loc}) \end{bmatrix} \quad (33a)$$

$${}^t\mathbf{K}_u = \int_V \mathbf{B}^T {}^t\mathbf{C}^{EP} \mathbf{B} dv \quad (33b)$$

where,

$$\begin{aligned} {}^{t+\Delta t}\mathbf{R} &= \int_S \mathbf{H}^T {}^{t+\Delta t}\mathbf{p} ds \\ {}^t\mathbf{F} &= \int_V \mathbf{B}^T {}^t\boldsymbol{\sigma} dv \end{aligned}$$

Following the same material evolution law already discussed in [D'heres and Dvorkin, 2009] we get,

$$\frac{\mathbf{\Theta}^T {}^{t+\Delta t}\mathbf{F}_{loc} - \mathbf{\Theta}^T {}^t\mathbf{F}_{loc}}{\mathbf{\Theta}^T {}^t\mathbf{F}_{loc}} = \frac{{}^{t+\Delta t}\sigma_{yloc} - {}^t\sigma_{yloc}}{{}^t\sigma_{yloc}} \quad (34)$$

Since the above equations correspond to the linearized step we have to iterate for solving the incremental step; using Newton iterations we get for the $n - th$ iteration,

$$\begin{bmatrix} {}^{t+\Delta t}\mathbf{K}_u^{(n-1)} & - {}^{t+\Delta t}\mathbf{K}_u^{(n-1)} \mathbf{\Theta} \\ - \mathbf{\Theta}^T {}^{t+\Delta t}\mathbf{K}_u^{(n-1)} & \mathbf{\Theta}^T {}^{t+\Delta t}\mathbf{K}_u^{(n-1)} \mathbf{\Theta} \end{bmatrix} \begin{bmatrix} \Delta\mathbf{U}^{(n)} \\ \Delta\gamma^{(n)} \end{bmatrix} = \begin{bmatrix} {}^{t+\Delta t}\mathbf{R} - {}^{t+\Delta t}\mathbf{F}^{(n-1)} \\ \mathbf{\Theta}^T ({}^{t+\Delta t}\mathbf{F}^{(n-1)} - {}^{t+\Delta t}\mathbf{F}_{loc}^{(n-1)}) \end{bmatrix} \quad (35a)$$

$${}^{t+\Delta t}\mathbf{K}_u^{(n-1)} = \int_V \mathbf{B}^T {}^{t+\Delta t}\mathbf{C}^{EP (n-1)} \mathbf{B} dv \quad (35b)$$

and,

$$\mathbf{U}^{(n)} = \mathbf{U}^{(n-1)} + \Delta\mathbf{U}^{(n)} \quad (36a)$$

$$[{}^{t+\Delta t}\gamma]^{(n)} = [{}^{t+\Delta t}\gamma]^{(n-1)} + \Delta\gamma^{(n)} \quad (36b)$$

The parameter $\Delta\gamma$ is condensed at the element level and the resulting stiffness matrix is symmetric.

3.3 Damage evolution

Let us consider a very simple damage model in which the evolution of the material yield stress is only function of the equivalent plastic strain. Hence,

$${}^t\sigma_y = {}^t\sigma_y ({}^t\bar{\varepsilon}^P). \quad (37)$$

A wide variety of much more involved material models that include plasticity and damage have been proposed in the literature, e.g. the Gurson-Tvergaard-Needleman material model, see [Gurson, 1975], [Gurson, 1977], [Tvergaard, 1981], [Tvergaard, 1982] and [Tvergaard and Needleman, 1981]; however, we use the above simple material model as a first test of our formulation for modeling localization problems with constitutive equations including damage evolution.

3.4 Length scale adoption

For the material inside the shear band we can specialize Eqn. (37) as,

$${}^t\sigma_{y_{loc}} = {}^t\sigma_{y_{loc}}({}^t\bar{\varepsilon}_{loc}^P). \quad (38)$$

It is important to recognize that Eqn. (21) is defined at the element scale and consistently models this scale (continuum scale); but, Eqn. (22) is defined at the element scale to model the localized deformations inside a band of very small or zero width. When considering a material that incorporates damage evolution, as for example the one in Eqn. (38), it is evident that the localized deformations must have a proper scale.

For the above purposes we postulate that the shear band equivalent plastic strain is proportional to the band incremental parameter γ through a positive inter-scales factor φ , which relates the continuum and localization scales,

$$(\bar{\varepsilon}_{loc}^P)^2 = \varphi^2 \gamma^2 \quad (39)$$

To determine φ we assume that all the energy dissipated by the localized mode is dissipated in the band volume (V_{loc}) during the deformation evolution,

$$\int_{t_\gamma}^{t+\Delta t_\gamma} \underline{\Theta}^T {}^t\mathbf{F}_{loc} d\gamma = \int_t^{t+\Delta t} \int_{V_{loc}} {}^t\sigma_{y_{loc}}(\bar{\varepsilon}_{loc}^P) d\bar{\varepsilon}_{loc}^P$$

using an Euler backward integration scheme we get,

$$\gamma \underline{\Theta}^T {}^{t+\Delta t}\mathbf{F}_{loc} = {}^{t+\Delta t}\sigma_{y_{loc}}(\bar{\varepsilon}_{loc}^P) \bar{\varepsilon}_{loc}^P h L \quad (40)$$

where h is a reference bandwidth and L is the band length along the element, as shown in Fig. 7.

Hence,

$$\varphi = \left| \frac{\underline{\Theta}^T {}^{t+\Delta t}\mathbf{F}_{loc}}{h L {}^{t+\Delta t}\sigma_{loc}(\bar{\varepsilon}_{loc}^P)} \right| \quad (41)$$

It must be noted that the parameter φ has to be recalculated at every iteration to ensure that Eqn. (40) is satisfied during the iterative scheme.

In our previous paper [D'heres and Dvorkin, 2009] we did not introduce a band scale and therefore when using it for material models including damage we do not have any available parameter to accommodate for different experimentally determined damage evolutions (Eqn. (38)); in the present paper we introduce the reference bandwidth - h - which can be used to phenomenologically model the observed material behavior. In Section 4 we will observe that for a material with the same damage evolution characterization (Eqn. (38)) by using different values of - h - we can reproduce different load-displacement paths.

3.5 Variables evolution

To model the evolution of the localization bands we need to keep track of the localization scale variables and of the continuous scale variables. For this purpose, we track, at the element center, the localization scale variables and, at the Gauss points, the continuous scale variables (Fig. 8).

Our algorithm for tracking the localization scale variables evolution at the element center can be summarized as follows:

1. Using the value of $\underline{\mathbf{U}}$ obtained from equilibrium iteration, we calculate the strain increment $\underline{\underline{\epsilon}}_c$ at the element center.
2. Starting from the converged values at time t and using the strain increment $\underline{\underline{\epsilon}}_c$ via the radial return algorithm ([Simo and Hughes, 1997]) we calculate at time $t + \Delta t$,

$$\underbrace{\underline{\underline{\epsilon}}_c, {}^t \underline{\underline{\epsilon}}_c, {}^t \underline{\underline{\epsilon}}_c^P, {}^t \sigma_{y_c}, {}^t \bar{\underline{\underline{\epsilon}}}_c^P}_{Input} \longrightarrow \boxed{\text{Radial return}} \longrightarrow \underbrace{{}^{t+\Delta t} \underline{\underline{\sigma}}_c, {}^{t+\Delta t} \sigma_{y_c}, \bar{\underline{\underline{\epsilon}}}_c^P}_{Output} \quad (42)$$

3. If there is an increment in $\bar{\underline{\underline{\epsilon}}}_c^P$ we are in the plastic loading regime; hence, the localization must be checked. Otherwise, the band remains closed and the continuum scale calculation is carried out with $\gamma = 0$.

For triggering the localization and for determining the band direction we use the converged values ${}^t \underline{\underline{\sigma}}_c$ and ${}^t \bar{\underline{\underline{\epsilon}}}_c^P$ and the test condition stated in Eqn. (13) if instantaneously ${}^t H < 0$.

For a developing band,

$$\varphi^{(i)} = \left| \frac{\underline{\underline{\Theta}}^T \quad {}^{t+\Delta t} \underline{\underline{\mathbf{F}}}_{loc}^{(i-1)}}{h \quad L \quad {}^{t+\Delta t} \sigma_{loc}^{(i-1)}} \right| \quad \text{and} \quad (\bar{\underline{\underline{\epsilon}}}_{loc}^P)^{(i)} = \varphi^{(i)} \gamma^{(i-1)},$$

and,

$${}^{t+\Delta t} \sigma_{y_{loc}}^{(i)} = {}^{t+\Delta t} \sigma_{y_{loc}} \left({}^t \bar{\underline{\underline{\epsilon}}}_{loc}^P + (\bar{\underline{\underline{\epsilon}}}_{loc}^P)^{(i)} \right).$$

Our algorithm for tracking the continuum scale variables evolution at the Gauss points can be summarized as follows:

1. At the Gauss points,

$$\underline{\underline{\epsilon}}_{cont} = \mathbf{B} (\underline{\underline{\mathbf{U}}} - \gamma \underline{\underline{\Theta}}) \quad (43)$$

2. Starting from the converged values at time t and using the strain increment $\underline{\underline{\epsilon}}_{cont}$ via the radial return algorithm we calculate at time $t + \Delta t$,

$$\underbrace{\underline{\underline{\epsilon}}, {}^t \underline{\underline{\epsilon}}, {}^t \underline{\underline{\epsilon}}^P, {}^t \sigma_y, {}^t \bar{\underline{\underline{\epsilon}}}^P}_{Input} \longrightarrow \boxed{\text{Radial return}} \longrightarrow \underbrace{{}^{t+\Delta t} \underline{\underline{\sigma}}, \bar{\underline{\underline{\epsilon}}}^P, \underline{\underline{\epsilon}}^P}_{Output} \quad (44)$$

4 Numerical implementation and some verification problems

The process of triggering in a finite element model the localization mechanism is not a smooth process and therefore it requires the adoption of some ad hoc smoothing techniques:

- Regarding the activation and deactivation of the band mechanism, every element is allowed to trigger-close it up to a number of times during a step (e.g. 4 to 8 times); if it exceeds this number, the opening of the band mechanism is precluded for the step.
- The global tangent stiffness matrix that results from the use of softening materials, may have negative eigenvalues when the band is established. Hence, in Eqn. (33a) the stiffness along the band direction $(\underline{\Theta}^T \ ^{t+\Delta t} \underline{\mathbf{K}}_u^{(n-1)} \ \underline{\Theta})$, may be too small and even negative; impairing therefore the algorithm convergence. In our numerical experimentation we stabilized the numerical convergence by closing the band during the iteration of the elements in which,

$$\underline{\Theta}^T \ ^{t+\Delta t} \underline{\mathbf{K}}_u^{(n-1)} \ \underline{\Theta} < k_{threshold}$$

with $k_{threshold}$ ranging from $\frac{1}{40}$ to $\frac{1}{10}$ of $(\underline{\Theta}^T \ ^{t+\Delta t} \underline{\mathbf{K}}_u^{(0)} \ \underline{\Theta})$. This stabilization procedure did not show to influence the analysis results.

4.1 Simple traction of a rectangular sheet under plane strain conditions

We depict the plane strain problem under consideration in Fig. 9 with $L = 8mm$. The sheet, with two symmetry planes, has a square notch to induce the localization. We imposed the displacements on the upper boundary and we continued the analysis up to an elongation of 4% or, we stopped it earlier, if ${}^t\sigma_y$ decreased below 10% of the initial ${}^0\sigma_y$.

We analyzed four different mesh densities,

Mesh	Horizontal Elem.	Vertical Elem.	Total Elem.
1	8	12	95
2	16	24	380
3	32	48	1520
4	64	96	6080

Table II. Regular meshes used to analyze the simple traction of a rectangular sheet

We analyzed the behavior of the QMITC element ([Dvorkin and Vassolo, 1989] - [Dvorkin et al., 1996]) and the Q2-P1 element [Bathe, 1996]; in both cases with the localization mechanism included in their formulation.

To show the mesh dependency of the solutions provided by elements with no ad hoc localization mechanism included in their formulation we used the standard QMITC element.

We considered the material parameters: $E = 200GPa$, ${}^0\sigma_y = 600MPa$, $\nu = 0.3$ and a softening tangent modulus of $E_T = -1GPa$. We adopted the damage law,

$${}^t\sigma_y = {}^0\sigma_y + E_T \ ^t\bar{\epsilon}^P. \quad (45)$$

4.1.1 Standard elements: mesh dependent solutions

The load displacement paths obtained using the standard QMITC element (without localization mechanism) are presented in Fig. 10, showing, as expected, mesh dependent results. The resulting equivalent plastic strain, ${}^t\bar{\varepsilon}^P$, is plotted in Fig. 11 where it can be observed that ${}^t\bar{\varepsilon}^P$ grows unbounded with mesh refinement overestimating therefore the material degradation, as discussed in [D’hers and Dvorkin, 2009]. To introduce an objective comparison criteria we plot, in Fig. 12, the energy dissipation predicted by this model. It can be seen that the dissipated energy slope grows unbounded with mesh refinement.

4.1.2 Our new formulation: mesh independent solutions

To elaborate on the behavior of the adopted lengthscale heuristic rule, we first compare the results obtained without a lengthscale as in [D’hers and Dvorkin, 2009] and those obtained when using a lengthscale related directly to the element area,

$$h L = A_{element}$$

We plot the load-displacement paths and the total energy dissipation predicted by the both models using different meshes in Figs. 13 and 14 respectively. Both models provide the same mesh independent results.

To show the ability of the formulation to represent different damage behaviors, we adopt $h = 0.1mm$ and $h = 0.05mm$ as bandwidth parameters and plot the resulting load-displacement curves in Figs. 15 and Fig. 16. In Fig 16. the different behavior observed between the meshes of 95 and 380 elements and the finer meshes of 1520 and 6080 elements is due to the fact that in the finner meshes two parallel bands open instead on a sigle one. This effect also happens in Fig 15. but it is less noticeable in the load displacement plot.

For each h -value the results are almost mesh independent and the unloading slope is controlled by the lengthscale. Hence, an experimental technique for determining the lengthscale for different materials and microstructures is available.

To complete the analysis, we plot in Fig. 17 the load-displacement curves corresponding to the regular and distorted meshes shown in Fig. 18; and in this figure we plot on the deformed configurations the corresponding equivalent plastic strains.

It is important to recognize that the lengthscale adoption implies that the energy is dissipated in an equivalent area,

$$h L = A_{localization}$$

defined by the h -parameter and, most important, that the parameter is not mesh dependent, that is to say, the parameter does need to be modified when using different element sizes.

Once the h -parameter has been set, the dissipated energy in the band is not unbounded and it converges with mesh refinement as it is shown in Fig. 19 for the case of QMITC elements including the localization mechanism in its kinematics.

4.1.3 Higher order elements

To show the behavior of our formulation when implemented with different elements, we plot in Fig. 20 the load displacement results obtained with the Q2-P1 element and in Fig. 21, we plot on the deformed

configuration the corresponding equivalent plastic strains. It can be seen that the obtained results are congruent for the different meshes.

5 CONCLUSIONS

This work follows our previous paper, [D'heres and Dvorkin, 2009], where we introduced the use of strong discontinuity modes to model shear bands localization.

In the present paper we introduce a lengthscale parameter (h -parameter) for heuristically modeling the material damage evolution inside the band. This h -parameter controls the damage-induced unloading behavior and therefore it can be determined, for different materials and microstructures, from actual experimental data. Hence, the defined lengthscale parameter is only dependent on the material behavior and therefore mesh independent.

The resulting formulation does not require a specific mesh refinement to model a localization, provides mesh independent results, allows the control of the downslope part of the load-displacement path via the h -parameter and the results are insensitive to element distortions.

Regarding the strong discontinuity modes that were initially developed for 4-node elements, we have extended them to higher order elements that are commonly used in the literature for modelling elastoplasticity.

This two-scale formulation does not introduce extra d.o.f. in the assembled numerical model and all the specific calculations are performed at element level.

Acknowledgement 1 *We gratefully acknowledge the support of TENARIS and ITBA for this research.*

6 References

References

- [Areias and Belytschko, 2006] Areias P.M.A. and Belytschko T., "Two-scale shear band evolution by local partition of unity", *Int. J. Numerical Methods in Engng.*, **66**, pp.878-910, 2006.
- [Armero and Garikipati, 1995] Armero F. and Garikipati K., "Recent Advances in the Analysis and Numerical Simulation of Strain Localization in Inelastic Solids", *Proc. Computational Plasticity COMPLAS IV*, (Ed. by D.R.J Owen, E. Oñate and E. Hinton), Barcelona, 1995.
- [Armero and Garikipati, 1996] Armero F. and Garikipati K., "Analysis of Strong Discontinuities in Multiplicative Finite Strain Plasticity and Their Relation with the Numerical Simulation of Strain Localization in Solids", *Int. J. Solids and Structures*, **33**, pp.2863-2885, 1996.
- [Armero, 2001] Armero F., "On the characterization of localized solutions in inelastic solids: an analysis of wave propagation in a softening bar", *Comput. Meth. Appl. Mech. Engng.*, **191**, pp.181-213, 2001.
- [Backofen, 1972] Backofen W. A., *Deformation Processing*, Addison-Wiley, 1972.

- [Bathe, 1996] Bathe K.-J., *Finite Element Procedures*, Prentice Hall, NJ, 1996.
- [Batisse et al., 1987] Batisse R., Bethmont M., Devesa G. and Rousselier G., "Ductile fracture of A 508 Cl 3 steel in relation with inclusion content: The benefit of the local approach of fracture and continuum damage mechanics", *Nuclear Engineering and Design*, **105**, pp.113-120, 1987.
- [Bažant, 1976] Bažant Z.P., "Instability, ductility and size effect in strain-softening concrete", *J. Engineering Mechanics(ASCE)* , **102**, pp.331–344, 1976; discussions, 1976; **103**, pp.357–358, 775–777; 1976; **104**, pp.501–502.
- [Belytschko et al., 1988] Belytschko T., Fish J. and Engelman E., "A finite element with embedded localization zones", *Comput. Meth. Appl. Mech. Engng.*, **70**, pp.59-89, 1988.
- [Belytschko et al., 2007] Belytschko T., Loehnert S. and Song J. H. "Multiscale aggregating discontinuities: A method for circumventing loss of material stability", *Int. J. Numerical Methods in Engng.*, pp.69-894, 2007.
- [Cervera et al., 2004] Cervera M., Chiumenti M. and Agelet de Saracibar C., "Shear band localization via local J2 continuum damage mechanics", *Comput. Methods Appl. Mech. Engng.*, **193**, pp.849–880, 2004.
- [D’hers and Dvorkin, 2009] D’hers S. and Dvorkin E.N., "Modeling shear bands in J2 plasticity using a two-scale formulation via embedded strong discontinuity modes", *Int. J. Numer. Meth. Engng.*, **77**, pp.1015–1043, 2009.
- [Dvorkin and Assanelli, 1991] Dvorkin E.N. and Assanelli A.P., "2D finite elements with displacement interpolated embedded localization lines: the analysis of fracture in frictional materials", *Comput. Meth. Appl. Mech. Engng.*, **90**, pp.829-844, 1991.
- [Dvorkin and Goldschmit, 2005] Dvorkin E.N. and Goldschmit M.B., *Nonlinear Continua*, Springer, Berlin, 2005
- [Dvorkin and Vassolo, 1989] Dvorkin E.N. and Vassolo S.I., "A quadrilateral 2D finite element based on mixed interpolation of tensorial components", *Engng. Computations*, **6**, pp.217-224, 1989.
- [Dvorkin et al., 1996] Dvorkin E.N., Assanelli A.P. and Toscano R.G., "Performance of the QMITC element in 2D elasto-plastic analyses", *Computers & Structures*, **58**, pp.1099-1129, 1996.
- [Dvorkin et al., 1990] Dvorkin E.N., Cuitiño A.M. and Gioia G., "Finite elements with displacement interpolated embedded localization lines insensitive to mesh size and distortions", *Int. J. Numerical Methods in Engng.*, **30**, pp.541-564, 1990.
- [Feyel and Chaboche, 2000] Feyel F. and Chaboche J.L., "FE2 multiscale approach for modelling the elastoviscoplastic behaviour of long fibre SiC/Ti composite materials", *Comput. Meth. Appl. Mech. Engng.*, **183**, pp.309–330. 2000.

- [Gilman, 1994] Gilman J.J., "Micromechanics of shear banding", *Mechanics of Materials*, **17**, pp.83–96, 1994.
- [Gurson, 1975] Gurson, A.L. "Plastic flow and fracture behavior of ductile materials incorporating void nucleation, growth and coalescence", Ph.D. thesis, Brown University, 1975.
- [Gurson, 1977] Gurson A.L., "Continuum theory of ductile rupture by void nucleation and growth: Part 1 - yield criteria and flow rules for porous ductile materials", *J. Eng. Matl. Tech.*, **99**, pp.2-15, 1977.
- [Hansbo and Hansbo, 2002] A. Hansbo and P. Hansbo, "An unfitted finite element method, based on Nitsche's method, for elliptic interface problems", *Comput. Meth. Appl. Mechs. Engng.*, **191**, pp.5537-5552, 2002.
- [Hansbo and Hansbo, 2004] Hansbo A. and Hansbo P., "A Finite Element method for the simulation of strong and weak discontinuities in elasticity", *Comput. Meth. Appl. Mechs. Engng.*, **193**, pp. 3523–3540, 2004.
- [Hutchinson and Tvergaard, 1981] Hutchinson, J.W. and Tvergaard, V., "Shear band formation in plane strain", *Int.J.Solids Struct.*, **17**, pp.451–470. 1981.
- [Ishikawa et al., 2000] Ishikawa N., Parks D.M. and Kurihara M., "Micromechanism of Ductile Crack Initiation in Structural Steels Based on Void Nucleation and Growth", *ISIJ International*, **40**, pp. 519–527, 2000.
- [Ishikawa et al., 2001] Ishikawa N., Parks D.M. and Kurihara M., "Micromechanical Modeling of Ductile Crack Initiation Behavior of Two Phase Steels", *ISIJ International*, **41**, pp. 76–85, 2001.
- [Larsson et al., 1993] Larsson R., Runesson K. and Ottosen N.S., "Discontinuum displacement approximation for capturing plastic localization", *Int. J. Num. Methods in Engng.*, **36**, pp.2087-2105, 1993.
- [Mergheim et al., 2005] Mergheim J., Kuhl E. and Steinmann P. , "A finite element method for the computational modelling of cohesive cracks", *Int. J. Numerical Methods in Engng.*, **63**, pp.276-289, 2005.
- [Mergheim et al., 2007] Mergheim J., Kuhl E. and Steinmann P., "Towards the algorithmic treatment of 3D strong discontinuities", *Communications in Numerical Methods in Engineering*, **23**, pp.97-108, 2007.
- [Moës et al., 1999] Moës N., Dolbow J. and Belytschko T., "A Finite Element Method for Crack Growth Without Remeshing", *Int. J. Numerical Methods in Engng.*, **46**, pp.131-150, 1999.
- [Needleman, 1989] Needleman A., "Dynamic shear band development in plane strain", *J. Appl. Mechs. (ASME)*, **56**, pp.1-9, 1989.

- [Oliver, 1996a] Oliver J., "Modeling strong discontinuities in solid mechanics via strain softening constitutive equations. Part 1: Fundamentals", *Int. J. Numerical Methods in Engng.*, **39**, pp.3575-3600, 1996.
- [Oliver, 1996b] Oliver J., "Modeling strong discontinuities in solid mechanics via strain softening constitutive equations. Part 2: Numerical simulation", *Int. J. Numerical Methods in Engng.*, **39**, pp.3601-3623, 1996.
- [Oliver and Huespe, 2004] Oliver J. and Huespe A.E., "Theoretical and computational issues in modelling material failure in strong discontinuity scenarios", *Comput. Meth. Appl. Mech. Engng.*, **193**, pp.2987-3014, 2004.
- [Oliver et al.,1999] Oliver J., Cervera M., Manzoli O., "Strong discontinuities and continuum plasticity models: the strong discontinuity approach", *International Journal of Plasticity*, **15**, pp.319–351, 1999.
- [Ortiz et al., 1987] Ortiz M., Leroy Y., Needleman A., "A Finite-Element Method for Localized Failure Analysis", *Comput. Meth. Appl. Mech. Engng.*, **61**, pp.189-214, 1987.
- [Ottosen, 1986] Ottosen N.S., "Thermodynamic consequences of strain softening in tension", *J. Eng. Mech. ASCE*, **112**, pp. 1152-1164, 1986.
- [Ottosen and Runesson, 1991] Ottosen N.S. and Runesson K., "Properties of discontinuum bifurcation solutions in elasto-plasticity". *Int. J. Solids Structures*, **27**, pp.401-421, 1991.
- [Rice, 1976] Rice J.R., "The Localization of Plastic Deformation", in *Theoretical and Applied Mechanics* (Proceedings of the 14th International Congress on Theoretical and Applied Mechanics, Delft, 1976, ed. W.T. Koiter), Vol. 1, North-Holland Publishing Co., pp.207-220, 1976.
- [Samaniego and Belytschko, 2005] Samaniego E. and Belytschko T., "Continuum–discontinuum modelling of shear bands", *Int. J. Numerical Methods in Engng.*,**62**, pp.1857-1872, 2005.
- [Sanchez et al., 2008] Sánchez P.J. ,Huespe A.E. and Oliver J., "On some topics for the numerical simulation of ductile fracture", *International Journal of Plasticity*, **24**, pp.1008–1038, 2008.
- [Simo et al., 1993] Simo J., Oliver J. and Armero F., "An analysis of strong discontinuities induced by strain-softening in rateindependent inelastic solids", *Computational Mechanics*, **12**, pp.277–296. 1993.
- [Simo and Hughes, 1997] Simo J.C. and Hughes T.J.R., *Computacional Inelasticity*, Springer, 1997.
- [Sluys, 1997] Sluys L.J., "Discontinuous modeling of shear banding", *Proc. Computational Plasticity COMPLAS V*, (Ed. by D.R.J Owen, E. Oñate and E. Hinton), Barcelona, 1997.

- [Tvergaard, 1981] Tvergaard, V., "Influence of voids on shear band instabilities under plane strain conditions", *Int. J. Fract.*, **17**, pp.389–407, 1981.
- [Tvergaard, 1982] Tvergaard, V., "On localization in ductile materials containing spherical voids", *Int. J. Fract.*, **18**, pp.237–252, 1982.
- [Tvergaard and Needleman, 1981] Tvergaard, V. and Needleman, A., "Analysis of the cup-cone fracture in a round tensile bar", *Acta Metall.* **32**, pp. 157–169, 1981.
- [Tvergaard et al., 1981] Tvergaard V., Needleman A. and Lo K.K., "Flow localization in the plane strain tensile test", *Journal of the Mechanics and Physics of Solids*, **29**, pp.115-142, 1981.
- [Yang et al., 2005] Yang Q., Mota A. and Ortiz M., "A class of variational strain-localization finite elements", *Int. J. Numerical Methods in Engng.*, **62**, pp.1013–1037, 2005.

Figure Captions:

1. Subdomains schematic representation
2. Band description
3. Bifurcation zones for various tH
4. Misalignment between maximum shear and bifurcation direction for ${}^tH = -0.1E$
5. Shear and volume change modes for a 9 node element
6. Continuum with an active localization
7. Scheme of a band in a localized element
8. Information storage scheme
9. Central notched specimen
10. Load-displacement without localization modes - QMITC
11. Equivalent plastic strain in the continuum without localization modes - QMITC
12. Energy dissipated in the band without localization modes - QMITC
13. Load-displacement with and without lengthscale - QMITC
14. Total energy dissipated in the band with and without lengthscale - QMITC
15. Load-displacement with $h=0.10$ - QMITC
16. Load-displacement with $h=0.05$ - QMITC
17. Load-displacement with $h=0.10$ for regular and distorted meshes - QMITC
18. Band equivalent plastic strain with $h=0.10$ for regular and distorted meshes - QMITC
19. Energy dissipated in the band with $h=0.10$ - QMITC
20. Load-displacement with $h=0.10$ for regular and distorted meshes - Q2P1
21. Band equivalent plastic strain with $h=0.10$ for regular and distorted meshes - Q2P1

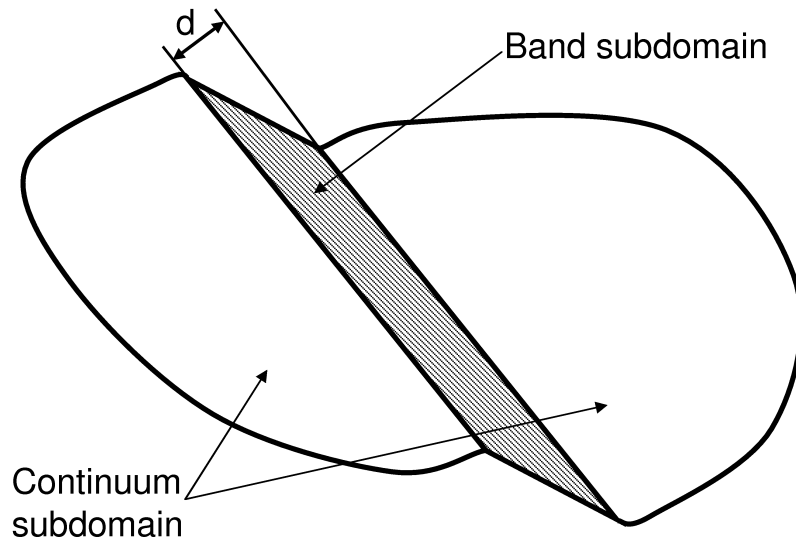


Fig. 1. Subdomains schematic representation

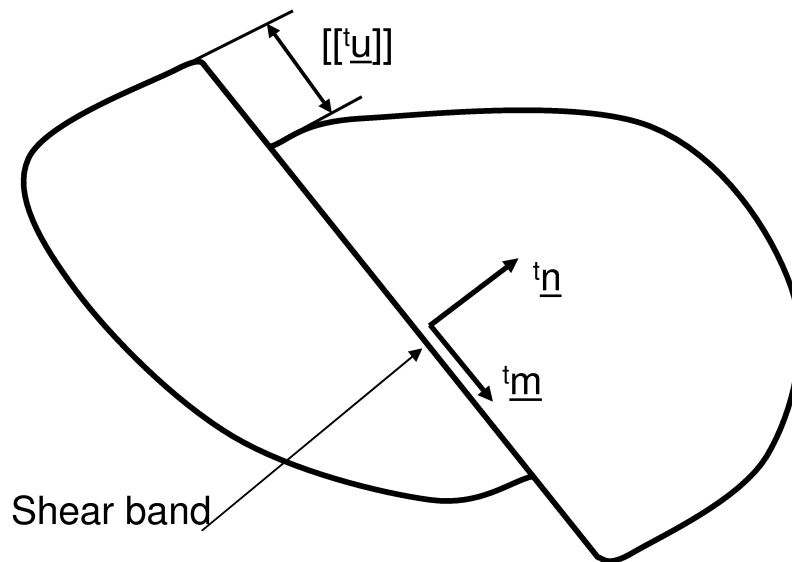


Fig. 2. Band description

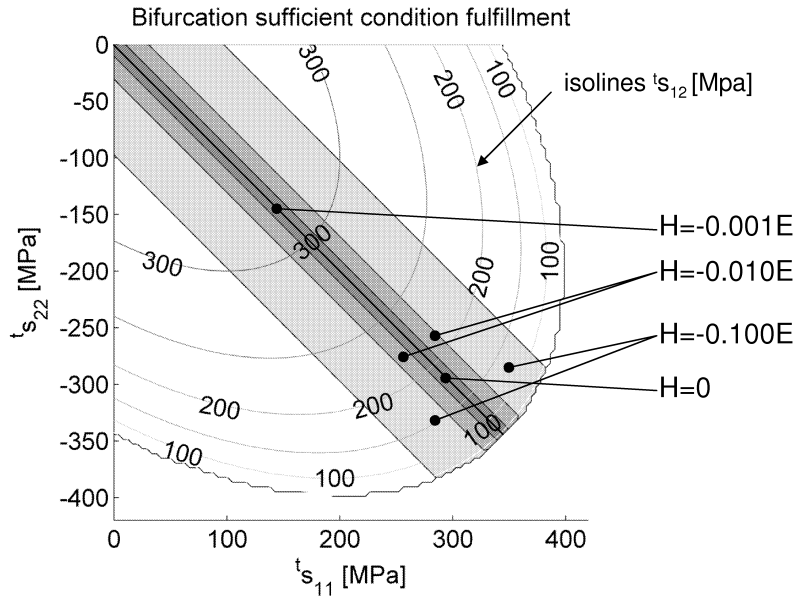


Fig. 3. Bifurcation zones for various tH

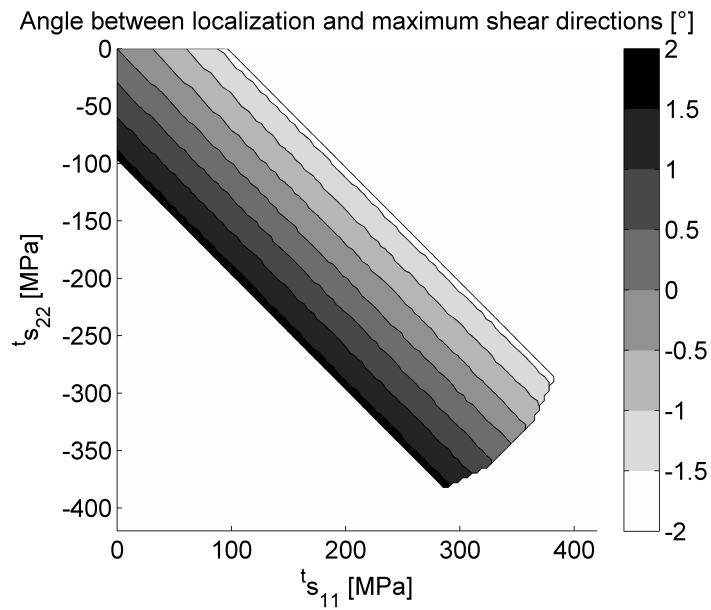


Fig. 4. Misalignment between maximum shear and bifurcation direction for $tH = -0.1E$

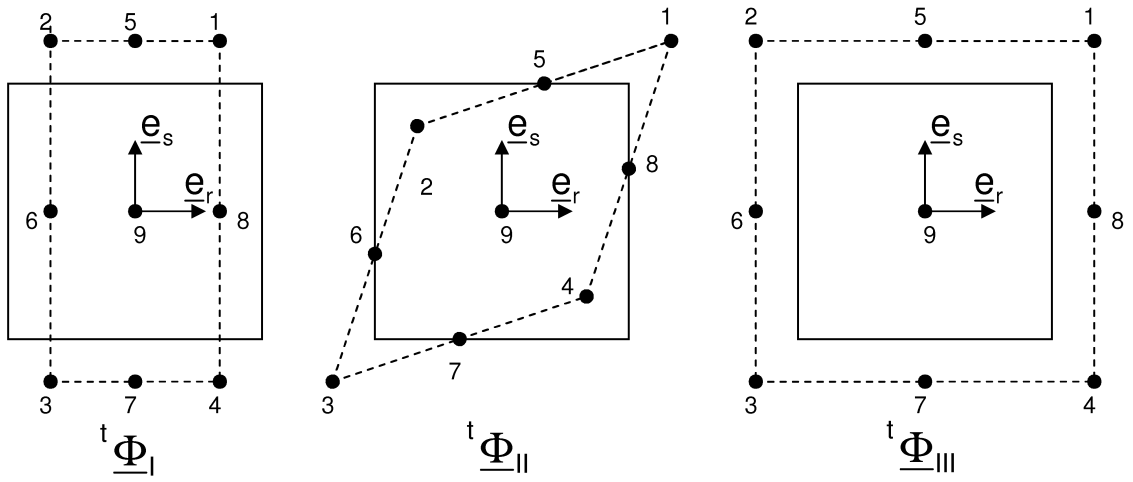


Fig. 5. Shear and volume change modes for a 9 node element

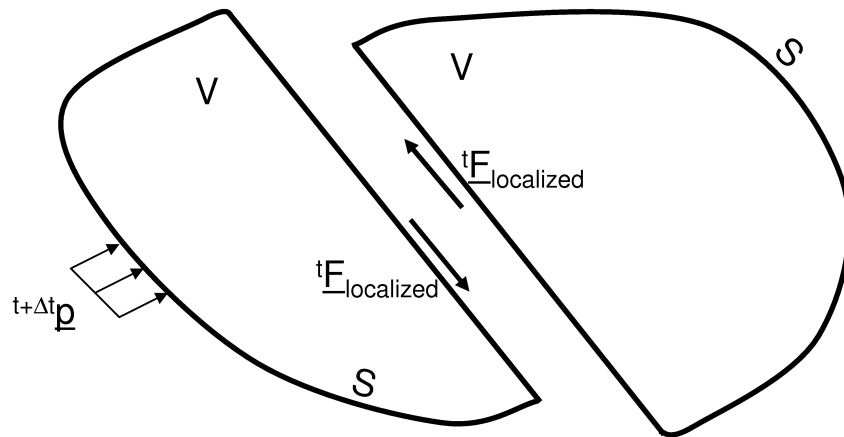


Fig. 6. Continuum with an active localization

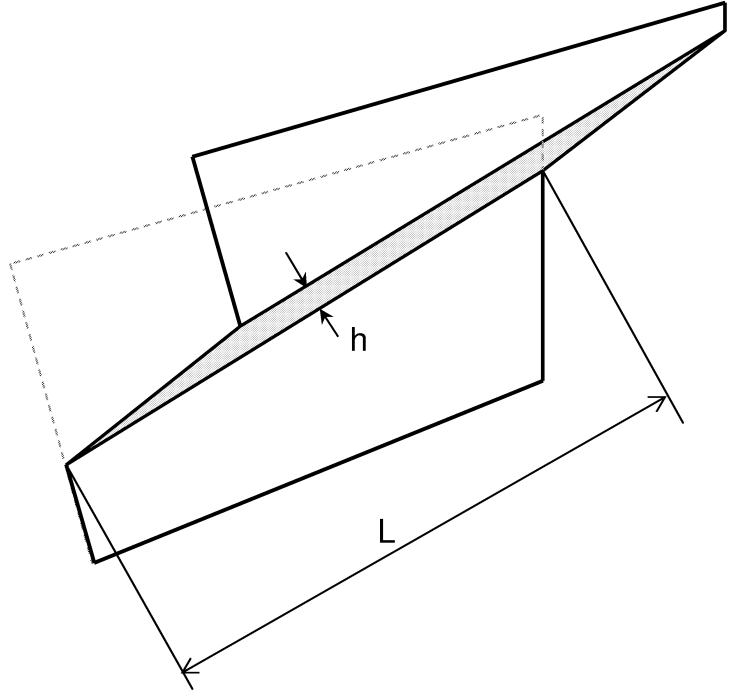


Fig. 7. Scheme of a band in a localized element

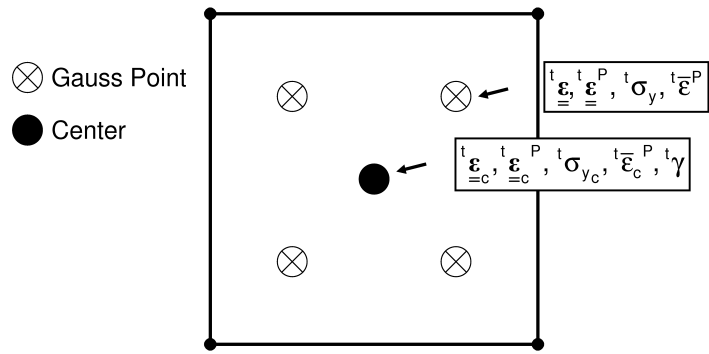


Fig. 8. Information storage scheme

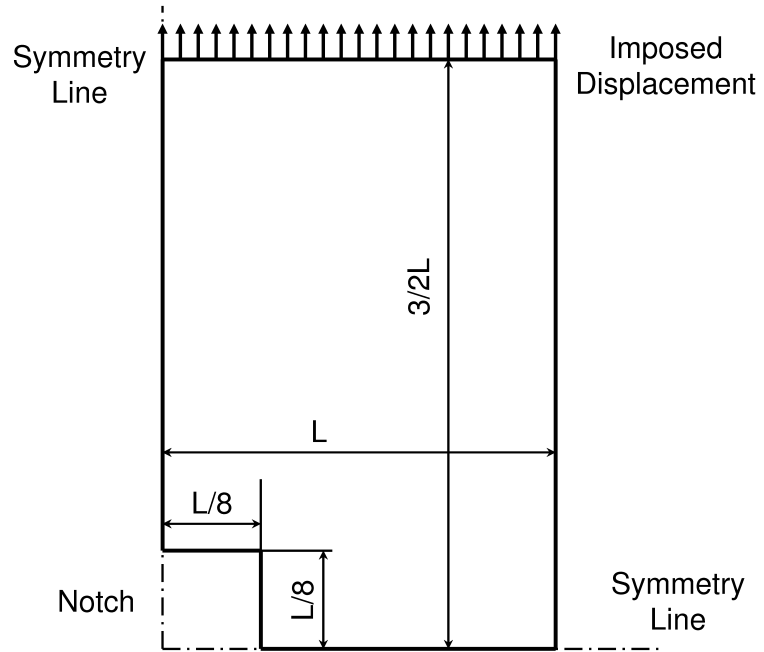


Fig. 9. Central notched specimen

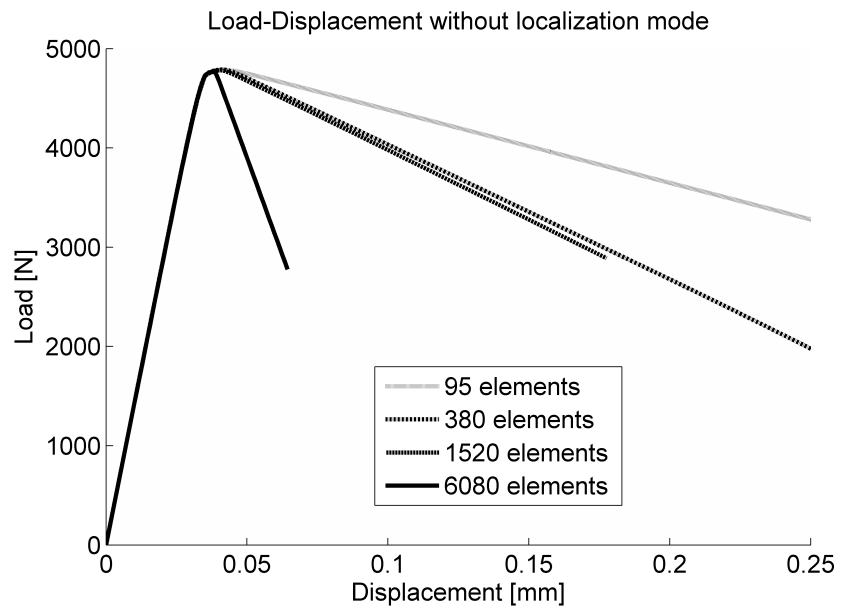


Fig. 10. Load-displacement without localization modes - QMITC

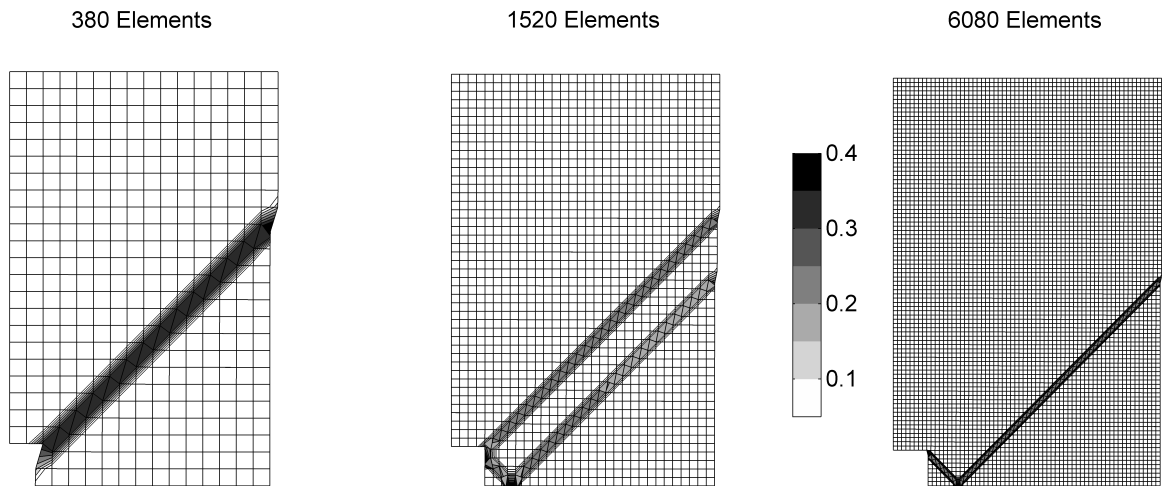


Fig. 11. Equivalent plastic strain in the continuum without localization modes - QMITC

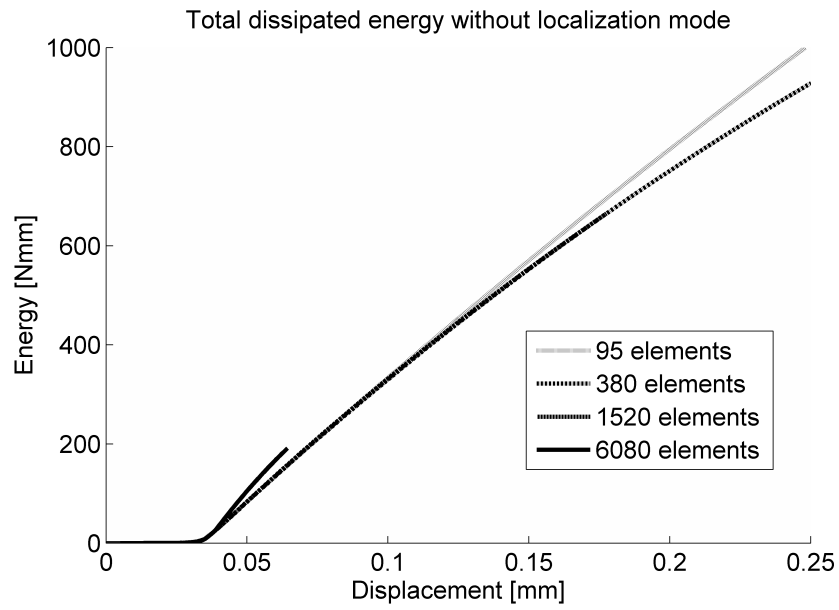


Fig. 12. Energy dissipated in the band without localization modes - QMITC

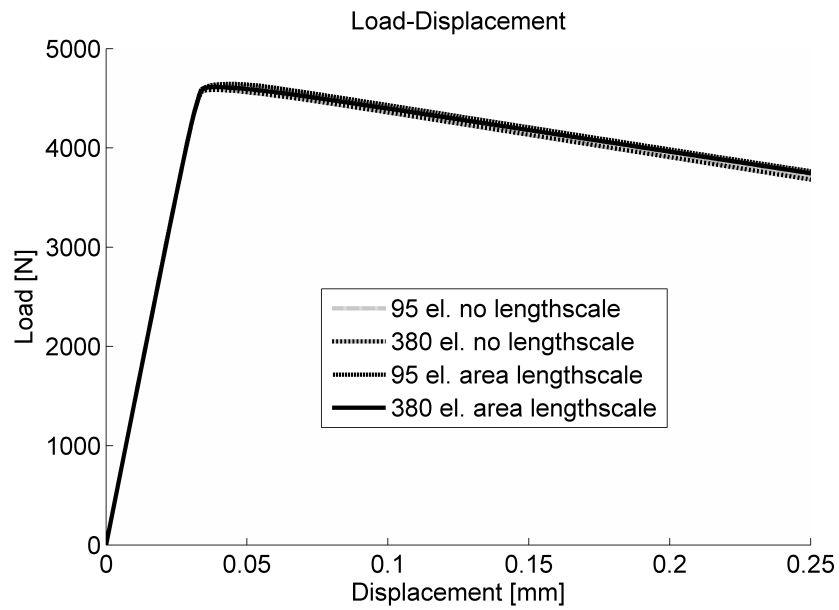


Fig. 13. Load-displacement with and without lengthscale - QMITC

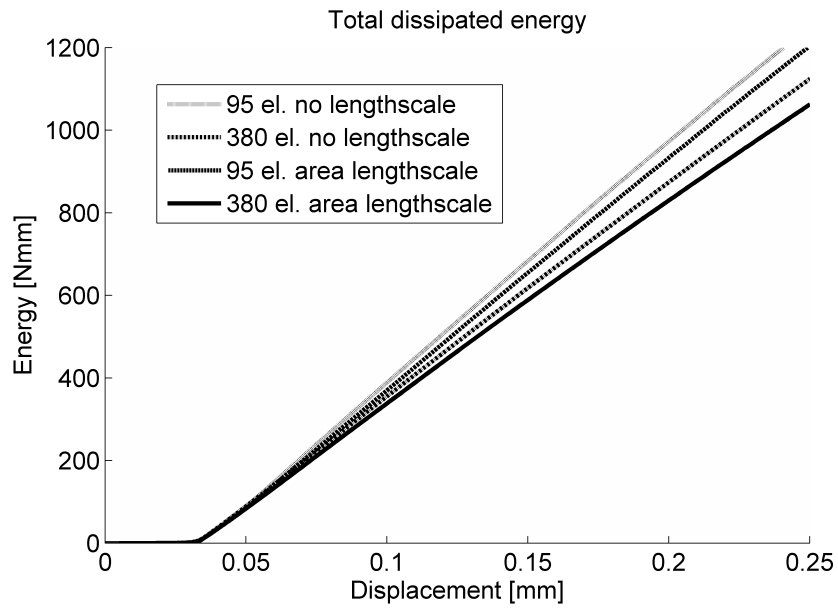


Fig. 14. Total energy dissipated in the band with and without lengthscale - QMITC

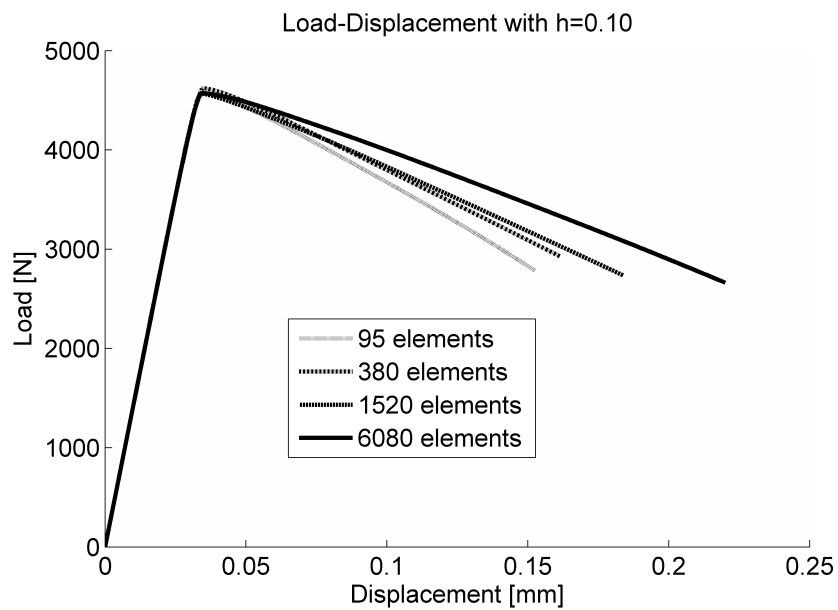


Fig. 15. Load-displacement with $h=0.10$ - QMITC

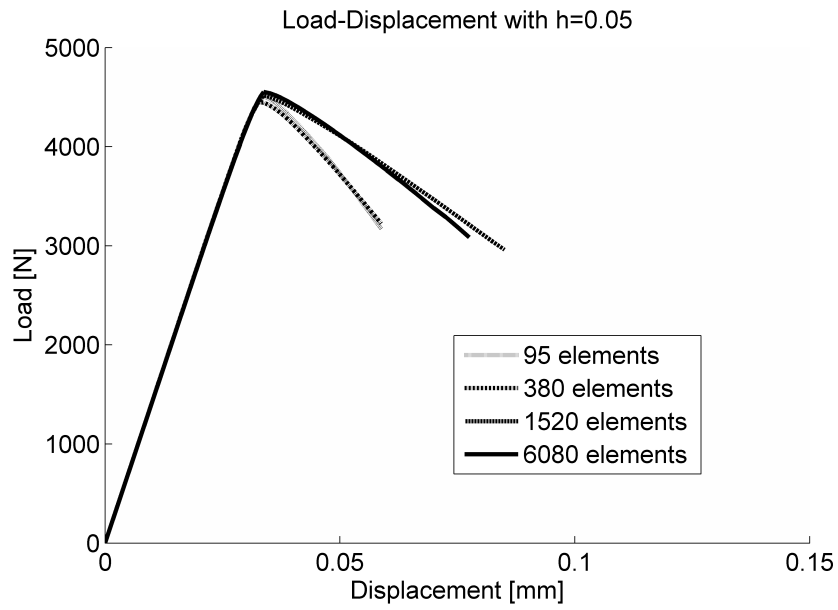


Fig. 16. Load-displacement with $h=0.05$ - QMITC

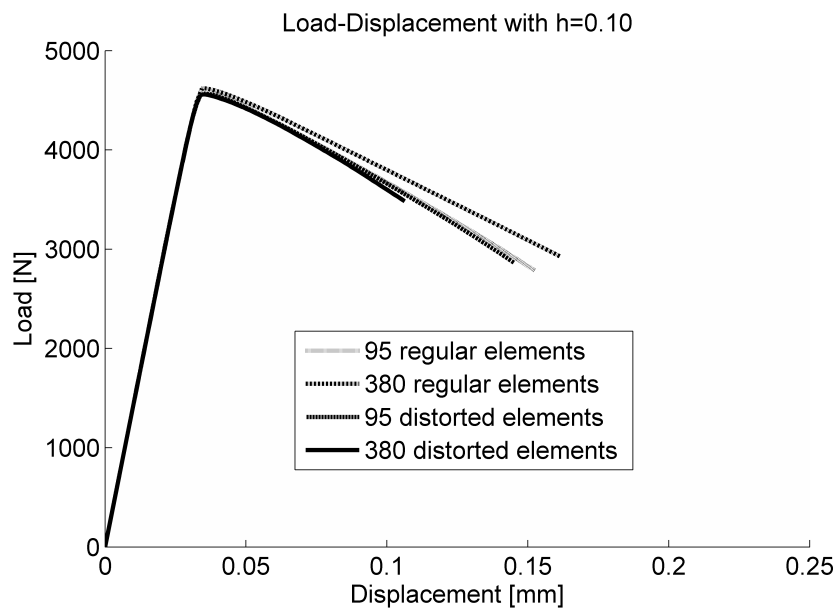


Fig. 17. Load-displacement with $h=0.10$ for regular and distorted meshes - QMITC

380 Regular elements

95 Distorted elements

380 Distorted elements

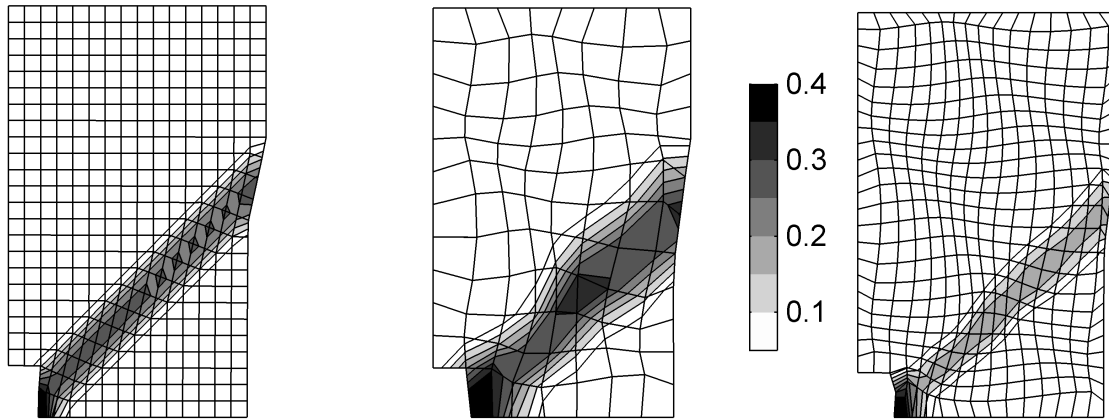


Fig. 18. Band equivalent plastic strain with $h=0.10$ for regular and distorted meshes - QMITC

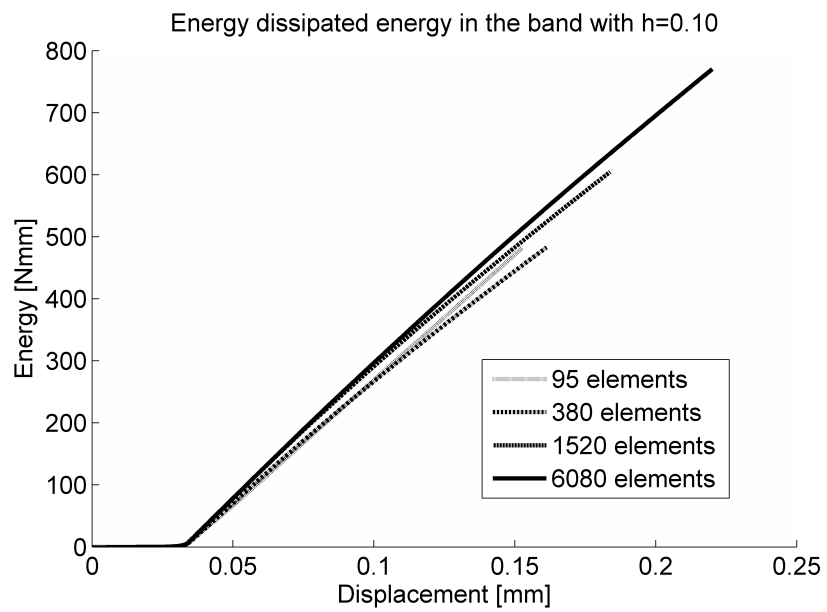


Fig. 19. Energy dissipated in the band with $h=0.10$ - QMITC

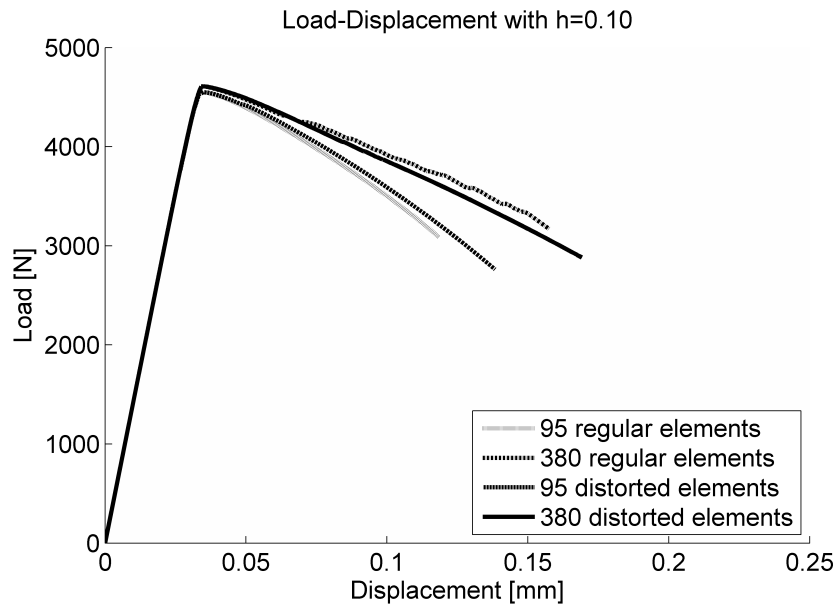


Fig. 20. Load-displacement with $h=0.10$ for regular and distorted meshes – Q2P1

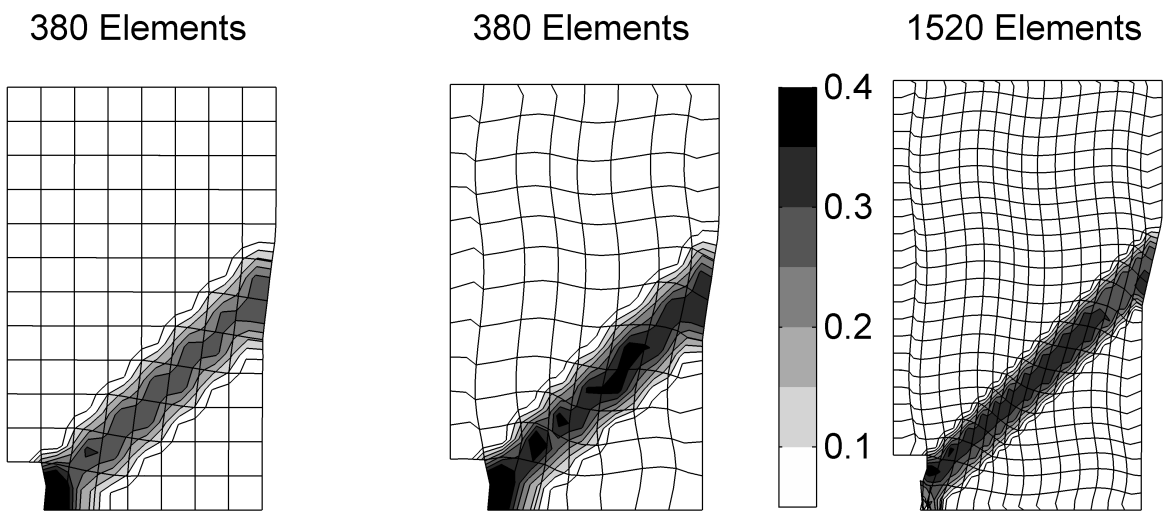


Fig. 21. Band equivalent plastic strain with $h=0.10$ for regular and distorted meshes – Q2P1